REIONIZATION OF THE UNIVERSE AND THE PHOTOEVAPORATION OF COSMOLOGICAL MINIHALOS

Paul R. Shapiro

University of Texas at Austin, USA

Alejandro C. Raga

Instituto de Astronomía, UNAM, México

RESUMEN

Las primeras fuentes de radiación ionizante que se condensaron del medio intergaláctico frío y neutro produjeron frentes de ionización que se propagaron en sus alredededores y alcanzaron a otras condensaciones, fotoevaporándolas. Aquí demostramos el efecto de esta retroalimentación de reionización sobre la formación de estructura cósmica, por medio de simulaciones hidrodinámicas que incluyen transporte radiativo para un minihalo cosmológico de materia oscura y bariones expuesto a una fuente externa de radiación ionizante (ya sea estelar o de cuasares), modelado justo después del paso del frente de radiación ionizante creado por la fuente.

ABSTRACT

The first sources of ionizing radiation to condense out of the dark and neutral IGM sent ionization fronts sweeping outward through their surroundings, overtaking other condensed objects and photoevaporating them. This feedback of universal reionization on cosmic structure formation is demonstrated here by gas dynamical simulations, including radiative transfer, for a cosmological minihalo of dark matter and baryons exposed to an external source of ionizing radiation, either starlight or quasar light, just after the passage of the global ionization front created by the source.

Key Words: **COSMOLOGY: THEORY — GALAXIES: FORMATION — HYDRODYNAMICS — INTERGALACTIC MEDIUM**

1. IONIZATION FRONTS IN THE IGM

The neutral, opaque IGM out of which the first bound objects condensed was dramatically reheated and reionized at some time between a redshift $z \approx 50$ and $z \approx 5$ by the radiation released by some of these objects. When the first sources turned on, they ionized their surroundings by propagating weak, R–type ionization fronts which moved outward supersonically with respect to both the neutral gas ahead of and the ionized gas behind the front, racing ahead of the hydrodynamical response of the IGM, as first described by Shapiro (1986) and Shapiro & Giroux (1987). These authors solved the problem of the time–varying radius of a spherical I–front which surrounds isolated sources in a cosmologically expanding IGM analytically, taking proper account of the I–front jump condition generalized to cosmological conditions. They applied these solutions to determine when the I–fronts surrounding isolated sources would grow to overlap and, thereby, complete the reionization of the universe. The effect of density inhomogeneity on the rate of I–front propagation was described by a mean "clumping factor" $c_l > 1$, which slowed the I–fronts by increasing the average recombination rate per H atom inside clumps. This suffices to describe the rate of I–front propagation as long as the clumps are either not self–shielding or, if so, only absorb a fraction of the ionizing photons emitted by the central source. Numerical radiative transfer methods are currently under development to solve this problem in 3D for the inhomogeneous density distribution which arises as cosmic structure forms, so far limited to a fixed density field without gas dynamics (e.g. Abel, Norman, & Madau 1999; Razoumov & Scott 1999; Ciardi et al. 2000). A
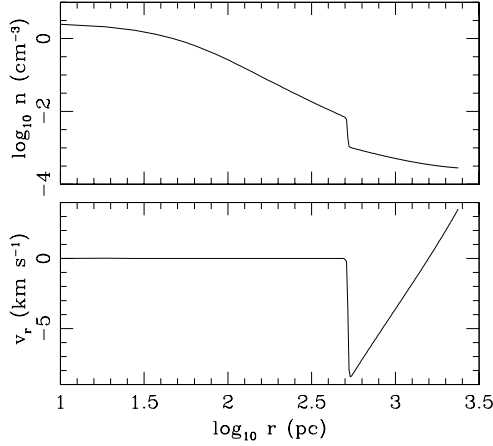
Fig. 1. MINIHALO INITIAL CON-
DITIONS BEFORE REIONIZATION.
(Top) gas density; (Bottom) gas veloc-
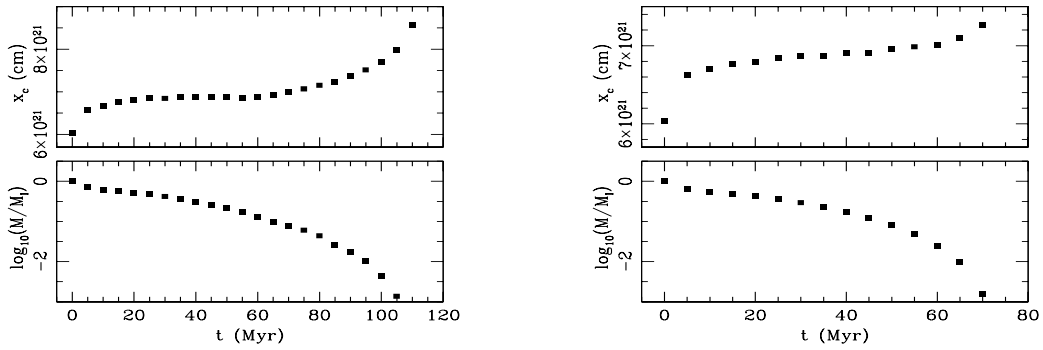ity versus distance from minihalo cen-
ter.

Fig. 2. I–FRONT PHOTOEVAPORATES MINIHALO: (upper panels) I–front position along x–axis versus
time; (lower panels) Mass fraction of the initial mass M_I of minihalo hydrostatic core which remains neutral
(H I) versus time.(a) (left) STELLAR CASE (b) (right) QUASAR CASE.

different, more approximate approach which is intended to mimic the average rate at which I–fronts expanded
and overlapped during reionization within the context of cosmological gas dynamics simulation has also been
developed (Gnedin 2000). The question of what dynamical effect the I–front had on the density inhomogeneities
it encountered, however, requires further analysis. Here we shall briefly summarize our results of the first
radiation–hydrodynamical simulations of the back–reaction of a cosmological I–front on a gravitationally bound
density inhomogeneity it encounters —a dwarf galaxy minihalo— during reionization.

2. THE PHOTOEVAPORATION OF DWARF GALAXY MINIHALOS OVERTAKEN BY A COSMOLOGICAL IONIZATION FRONT

We have performed radiation–hydrodynamical simulations of the photoevaporation of a cosmological mini-
halo overrun by a weak, R–type I–front in the surrounding IGM, created by an external source of ionizing
radiation (Shapiro & Raga 2000a,b). Our simulations in 2D, assuming axisymmetry used an Eulerian hydro
code with Adaptive Mesh Refinement and the Van Leer flux–splitting algorithm, which solved nonequilibrium
ionization rate equations (for H, He, C, N, O, Ne, and S) and included an explicit treatment of radiative transfer
by taking into account the bound–free opacity of H and He. A possible heavy element abundance of 10^{-3} times
solar was assumed, as well.

Here we compare some of those results for two different sources: a quasar–like source with emission spectrum
$F_\nu \propto \nu^{-1.8}$ ($\nu > \nu_H$) and a stellar source with a 50,000 K blackbody spectrum, with luminosity and distance
adjusted to keep the ionizing photon fluxes the same in the two cases. In particular, if r_{Mpc} is the distance
(in Mpc) between source and minihalo and $N_{\mathrm{ph},56}$ is the H–ionizing photon luminosity (in units of $10^{56}\,s^{-1}$),
then the flux at the location of the minihalo would, if unattenuated, correspond to $N_{\mathrm{ph},56}/r_{\mathrm{Mpc}}^2 = 1$.   Our
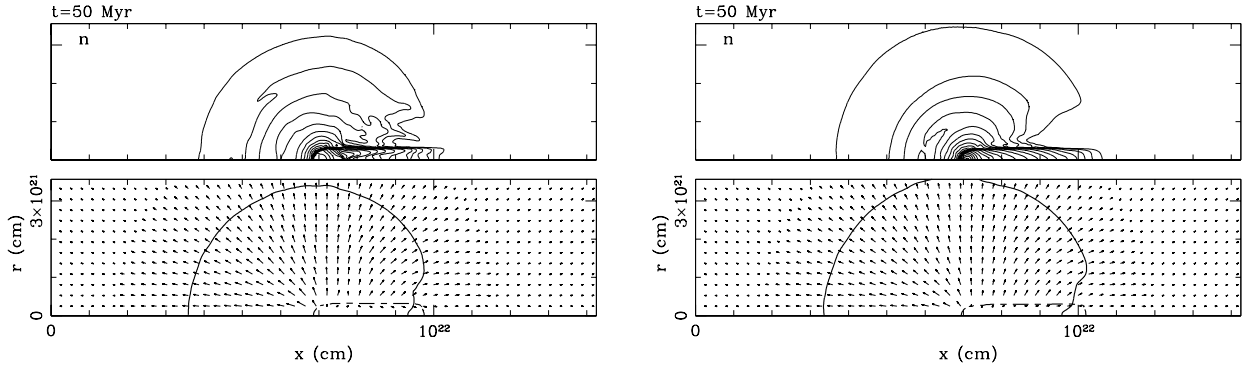
Fig. 3. PHOTOEVAPORATING MINIHALO: One time–slice 50 Myr after turn–on of ionizing source to the left of computational box along the x–axis. (a) (left) STELLAR CASE. (upper panel) isocontours of atomic density, logarithmically spaced, in $(r, x) - -$plane of cylindrical coordinates; (lower panel) velocity arrows are plotted with length proportional to gas velocity. An arrow of length equal to the spacing between arrows has velocity $25\,\mathrm{km\,s^{-1}}$. Solid line shows current extent of gas originally in hydrostatic core. Dashed line is I–front (50% H–ionization contour). (b) (right) QUASAR CASE. Same as (a), except for quasar source, instead, and an arrow of length equal to the spacing between arrows has velocity $30\,\mathrm{km\,s^{-1}}$.

initial condition before ionization, shown in Figure 1, is that of a $10^7 M_\odot$ minihalo in an Einstein–de Sitter universe ($\Omega_{\mathrm{CDM}} = 1 - \Omega_{\mathrm{bary}}$; $\Omega_{\mathrm{bary}} h^2 = 0.02$; $h = 0.7$) which collapses out and virializes at $z_{\mathrm{coll}} = 9$, yielding a truncated, nonsingular isothermal sphere of radius $R_c = 0.5\,\mathrm{kpc}$ in hydrostatic equilibrium with virial temperature $T_{\mathrm{vir}} = 5900\,\mathrm{K}$ and dark–matter velocity dispersion $\sigma_V = 6.3\,\mathrm{km\,s^{-1}}$, according to the solution of Shapiro, Iliev, & Raga (1999), for which the finite central density inside a radius about $1/30$ of the total size of the sphere is 514 times the surface density. This hydrostatic core of radius R_c is embedded in a self–similar, spherical, cosmological infall according to Bertschinger (1985).

The results of our simulations on an (r, x)–grid with 256×512 cells (fully refined), summarized in Figures 2–6, include the following points:

- The background IGM and infalling gas outside the minihalo [centered at $(r, x) = (0, 7.125 \times 10^{21}\,\mathrm{cm})$] are quickly ionized, and the resulting pressure gradient in the infall region converts the infall into an outflow.

- As expected, the hydrostatic core of the minihalo shields itself against ionizing photons, trapping the I–front which enters the halo, causing it to decelerate inside the halo to the sound speed of the ionized gas before it can exit the other side, thereby transforming itself into a weak, D–type front preceded by a shock.

- The side facing the source expels a supersonic wind backwards towards the source, which shocks the IGM outside the minihalo, while the remaining neutral halo material is accelerated away from the source by the so–called "rocket effect" as the halo photoevaporates (cf. Spitzer 1978). Since this is a case of gas bound to a dark halo with $\sigma < 10\,\mathrm{km\,s^{-1}}$, this photoevaporation proceeds unimpeded by gravity.

- Figures 2(a) and (b) show the position of the I–front inside the minihalo as it slows from weak, R–type to weak D–type led by a shock as it advances across the original hydrostatic core, for the two cases. Figures 2(a) and (b) also show the mass of the neutral zone within the original hydrostatic core shrinking as the minihalo photoevaporates within about 100 Myrs. The photoevaporation time is 50 % larger for the stellar source than for the quasar source.

- Figures 3 and 4 show the structure of the photoevaporative flow 50 Myrs after the global I–front first overtakes the minihalo, with key features of the flow indicated by the labels on the temperature plot in Figure 4. For the stellar case, a strong shock labelled "4S" clearly leads the D-type I–front (labelled
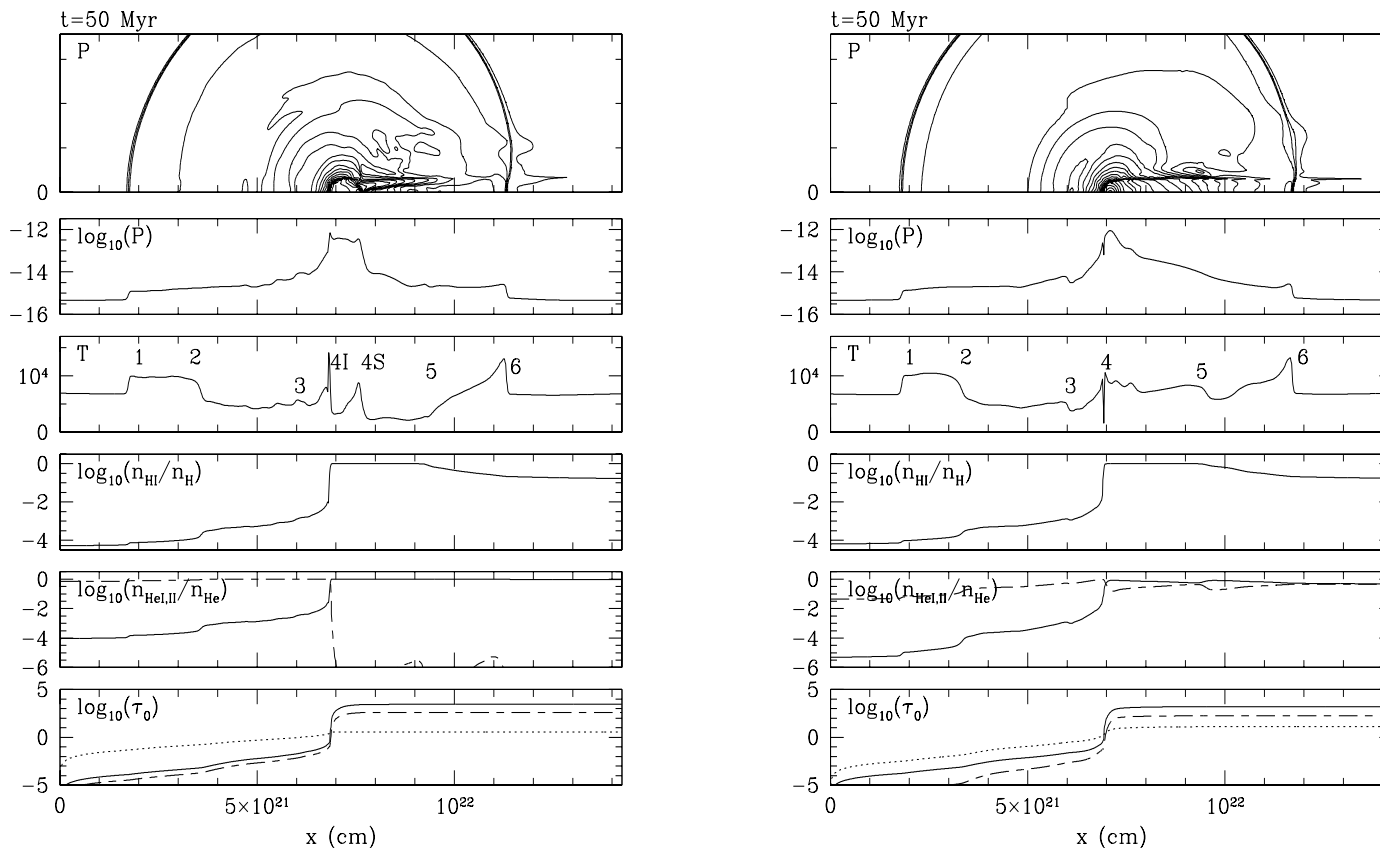
Fig. 4: PHOTOEVAPORATING MINIHALO: One time–slice 50 Myr after turn–on of ionizing source located to the left of computational box along the x–axis. (a) (left) STELLAR CASE. From top to bottom: (i) isocontours of pressure, logarithmically spaced, in (r, x)–plane of cylindrical coordinates; (ii) pressure along the $r = 0$ symmetry axis; (iii) temperature; (iv) H I fraction; (v) He I (solid) and He II (dashed) fractions; (vi) bound–free optical depth along $r = 0$ axis at the threshold ionization energies for H I (solid), He I (dashed), He II (dotted). Key features of the flow are indicated by the numbers which label them on the temperature plot: 1 = IGM shock; 2 = contact discontinuity between shocked halo wind and swept–up IGM; 3 = wind shock; between 3 and 4 = supersonic wind; 4I = I–front; 4S = shock which precedes I–front; 5 = boundary of gas originally in hydrostatic core; 6 = shock in shadow region caused by compression of shadow gas by shock–heated gas outside shadow. (b) (right) QUASAR CASE. Same as (a), except for quasar source, instead, and label 4 = I–front in temperature plot.
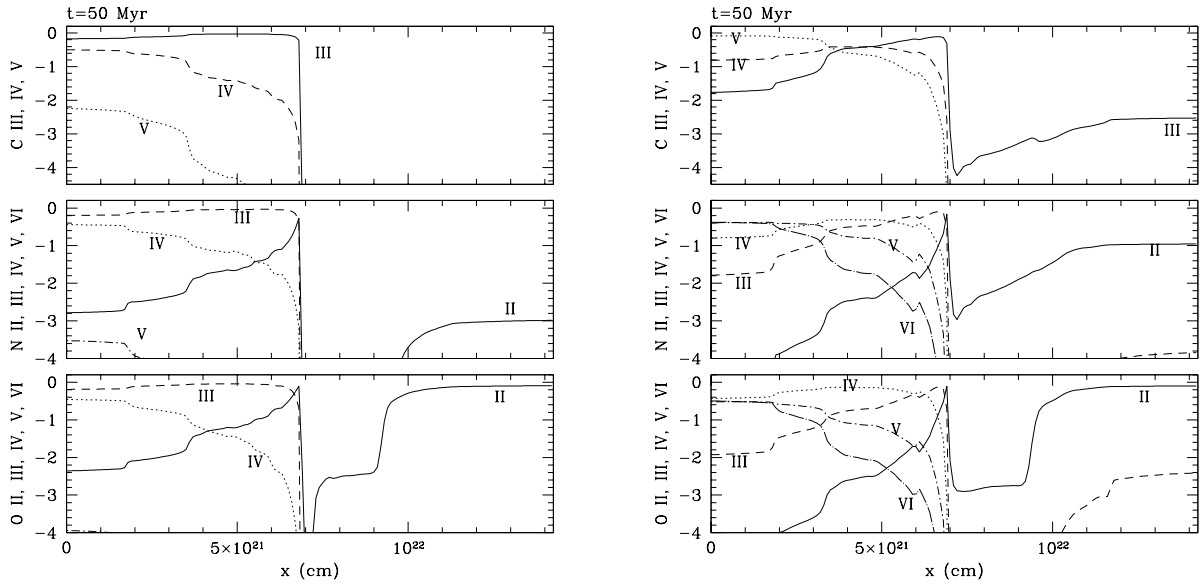
Fig. 5. OBSERVATIONAL DIAGNOSTICS I: IONIZATION STRUCTURE OF METALS. C, N, and O ionic fractions along symmetry axis at $t = 50$ Myr. (a) (left) STELLAR CASE; (b) (right) QUASAR CASE
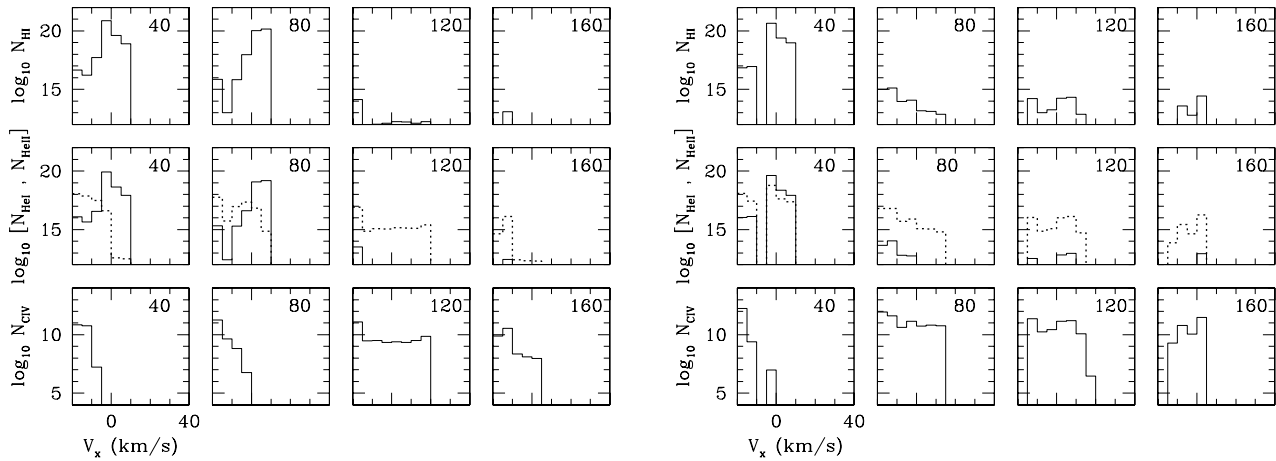
Fig. 6. OBSERVATIONAL DIAGNOSTICS II. ABSORPTION LINES. Minihalo column densities (cm^{-2}) along symmetry axis at different velocities. (Top) H I; (Middle) He I (solid) and He II (dotted); (Bottom) C IV. Each box labelled with time (in Myrs) since source turn–on. (a) (left) STELLAR CASE; (b) (right) QUASAR CASE.

"4I") as it advances through the minihalo core, by contrast with the quasar case in which hard photons penetrate deeper into the neutral gas and preheat it, thereby weakening the shock which leads the I–front. The softer stellar spectrum also explains why helium on the ionized side of the I–front is mostly He II, rather than He III as in the quasar case, while the neutral side is completely He I, rather than a mix of He I and II as in that case.

- Figure 5 shows the spatial variation of the relative abundances of C, N, O ions along the symmetry axis after 50 Myrs. While the quasar case shows the presence at 50 Myrs of low as well as high ionization stages for the metals, the softer spectrum of the stellar case yields less highly ionized gas on the ionized side of the I–front (e.g. mostly C III, N III, O III) and the neutral side as well (e.g. C II, N I, O I and II).

- The column densities of H I, He I and II, and C IV for minihalo gas of different velocities as seen along the symmetry axis at different times are shown in Figure 6. At early times, the minihalo gas resembles a weak Damped Lyman α ("DLA") absorber with small velocity width ($\geq 10\,\mathrm{km\,s^{-1}}$) and $N_{\mathrm{H\,I}} \geq 10^{20}\mathrm{cm}^{-2}$, with a Lyman–$\alpha$–Forest("LF")-like red wing (velocity width $\geq 10\,\mathrm{km\,s^{-1}}$) with $N_{\mathrm{H\,I}} \geq 10^{16}\mathrm{cm}^{-2}$ on the side moving toward the source, with a He I profile which mimics that of H I but with $N_{\mathrm{He\,I}}/N_{\mathrm{H\,I}} \sim [\mathrm{He}]/[\mathrm{H}]$, and with a weak C IV feature with $N_{\mathrm{C\,IV}} \sim 10^{11}\,(10^{12})\,\mathrm{cm}^{-2}$ for the stellar (quasar) cases, respectively, displaced in this same asymmetric way from the velocity of peak H I column density. For He II at early times, the stellar case has $N_{\mathrm{He\,II}} \approx 10^{18}\mathrm{cm}^{-2}$ shifted by tens of km/s to the red of the H I peak, while for the quasar case, He II simply follows the H I profile, except that $N_{\mathrm{He\,II}}/N_{\mathrm{H\,I}} \approx 10$ in the red wing but $N_{\mathrm{He\,II}}/N_{\mathrm{H\,I}} \approx 10^{-2}$ in the central H I feature. After 160 Myr, however, only a narrow H I feature with LF-like column density $N_{\mathrm{H\,I}} \sim 10^{13}\,(10^{14})\mathrm{cm}^{-2}$ remains, with $N_{\mathrm{He\,I}}/N_{\mathrm{H\,I}} \sim 1/4\,(< 1/10)$, $N_{\mathrm{He\,II}}/N_{\mathrm{H\,I}} \sim 10^3\,(10^2)$, and $N_{\mathrm{C\,IV}}/N_{\mathrm{H\,I}} \sim 3[\mathrm{C}]/[\mathrm{C}]_\odot\,([\mathrm{C}]/[\mathrm{C}]_\odot)$ for the stellar (quasar) cases, respectively.

- Observations of the absorption spectra of high redshift sources like those which reionized the universe may reveal the presence of photoevaporative flows like these and provide a useful diagnostic of the reionization process.

- Future work will extend this study to minihalos of higher virial temperatures, for which gravity competes more effectively with photoevaporation.

REFERENCES

Abel, T., Norman, M. L. & Madau, P. 1999, ApJ, 523, 66
Bertschinger, E. 1985, ApJS, 58, 39
Ciardi B., Ferrara A., Marri S. & Raimondo G. 2000, astro-ph/0005181
Gnedin, N. 2000, ApJ, 535, 530
Razoumov, A. & Scott, D. 1999, MNRAS, 309, 287
Shapiro, P. R. 1986, PASP, 98, 1014
Shapiro, P. R. & Giroux, M. L. 1987, ApJ, 321, L107
Shapiro, P. R., Iliev, I. T. & Raga, A. C. 1999, MNRAS, 307, 203
Shapiro, P. R. & Raga, A. C. 2000a, in Astrophysical Plasmas: Codes, Models and Observations, eds. S. J. Arthur, N. Brickhouse, & J.J. Franco, RevMexAA (SC), 9, 292 (astro-ph/0002100)
Shapiro, P. R. & Raga, A. C. 2000b, in Cosmic Evolution and Galaxy Formation: Structure, Interactions, and Feedback, ASP Conference Series, eds. J. Franco, E. Terlevich, O. López-Cruz, I. Aretxaga, in press (astro-ph/0004413)
Spitzer, L. 1978, Physical Processes in the Interstellar Medium (NY: Wiley)

Paul R. Shapiro, Dept. of Astronomy, University of Texas, Austin, TX 78712 (shapiro@astro.as.utexas.edu)
Alejandro C. Raga, Instituto de Astronomía, UNAM, Apartado Postal 70-264, 04510 México D. F., México (raga@astroscu.unam.mx).